Applied Catalysis B: Environmental 111–112 (2012) 433–444

Contents lists available at SciVerse ScienceDirect

Applied Catalysis B: Environmental

journal homepage: www.elsevier.com/locate/apcatb

NO_2 adsorption on Fe- and Cu-zeolite catalysts: The effect of the catalyst red–ox state

Massimo Colombo, Isabella Nova, Enrico Tronconi*

Laboratory of Catalysis and Catalytic Processes, Dipartimento di Energia, Politecnico di Milano, Piazza Leonardo da Vinci 32, 20133 Milano, Italy

ARTICLE INFO

Article history:
Received 1 July 2011
Received in revised form 19 October 2011
Accepted 21 October 2011
Available online 7 November 2011

Keywords:
Adsorption
Diesel exhaust aftertreatment
Nitrogen oxides
Urea SCR
Zeolite catalysts

ABSTRACT

In the present work we investigate the adsorption of NO_2 onto a Fe- and a Cu-promoted zeolite SCR catalyst in the absence of gaseous water, with a particular focus on the effect of the catalyst red–ox state. For both catalytic systems, results from the analysis of the gas phase during step changes of the NO_2 concentration, combined with literature FTIR information, emphasize an important role of the catalyst red–ox state in the dynamics of NO_2 adsorption: the molar ratio of released NO to adsorbed NO_2 is close to 1/3 in the case of oxidized catalysts, in line with a two-steps mechanism leading to the formation of surface nitrates, but is greater when the catalyst is partially reduced. Furthermore the initial catalyst red–ox state influences the amount of nitrates that can be adsorbed on the catalyst surface, the pre-reduced sample exhibiting a greater storage capacity. The Cu-zeolite catalysts are able to store a greater amount of nitrates and are more easily reduced in comparison with the Fe-zeolite.

1. Introduction

In the last decades the consciousness of the damages to environment and human health caused by gas emissions from combustion sources has grown significantly worldwide. Several air pollutants are now continuously monitored and their emissions have been regulated in many countries, including carbon oxides (CO_x), nitrogen oxides (NO_x), particulate matter (PM), sulphur oxides (SO_x) and volatile organic compounds (VOC).

As more and more stringent emission standards are introduced to lower the concentrations of such polluting agents in the atmosphere [1], the research has been driven towards the development of either low emission processes or systems for pollutants abatement.

Focusing on nitrogen oxides, their direct reduction from the exhaust gases of lean combustion engines [1,2] as well as their removal from ambient air [3] has attracted a great deal of attention in recent years. Different solutions (e.g. selective catalytic reduction (SCR) of NO_x by ammonia/urea and lean NO_x traps (LNT)) have been developed and commercially applied for the direct reduction of NO_x emitted from diesel engines [1], but also the removal of NO_x from ambient air has led to the development of different technologies (e.g. photocatalytic technologies) [4–6].

Particularly focusing on NO_2, it is interesting to notice that, among the several different materials able to interact with this molecule (e.g. alumina [7,8] and titania [9]), transition-metal exchanged zeolites have been proposed for both NO_2 adsorption from ambient air [3] and NO_2 reduction in an oxygen-rich environment [1,10]. A relevant number of studies regarding the interaction of NO_2 with different zeolite systems can be traced in the past and recent scientific literature. Most of these studies were carried out using FTIR techniques, which clearly supported the formation of stable surface nitrates upon exposure to NO_2 [10–17]; other works have also focused on the analysis of the temperature programmed desorption (TPD) of such adsorbed nitrate species, in order to investigate their thermal stability [11,13,18–20].

The mechanism of NO_2 interaction with metal-promoted zeolites to form surface nitrate species, however, is still debated. The purpose of the present work is thus to analyse such a mechanism over two commercial Fe- and Cu- promoted zeolite SCR catalysts, tested as crushed monolith powders. Results from the temporal analysis of the gas phase during step changes in the NO_2 concentration, combined with literature FTIR information, emphasize an important role of the catalyst red–ox state in the dynamics of NO_2 adsorption, which has been so far overlooked, and possibly explains some contradictions apparent in recent literature reports. This is indeed the first report focused on the analysis of the gas-phase products evolution during NO_2 adsorption onto catalysts associated with different red–ox states.

2. Experimental

Data presented in this work were obtained using an experimental setup specifically designed to perform transient kinetic runs over powdered catalysts [21].

* Corresponding author. Tel.: +39 02 2399 3264; fax: +39 02 2399 3318.
E-mail address: enrico.tronconi@polimi.it (E. Tronconi).

0926-3373/$ – see front matter © 2011 Elsevier B.V. All rights reserved.
doi:10.1016/j.apcatb.2011.10.031

Two commercial metal promoted zeolite catalysts, namely a Fe-BEA and a Cu-CHA, were investigated in the present study. They were originally received in the form of cordierite honeycomb monoliths (400 cpsi) washcoated with the zeolite-based active phase. More details about catalysts properties can be found in Refs. [22,23]. Before the tests, the original monolith catalysts were crushed and sieved to 140–200 mesh.

Samples of catalyst powder (60 mg for the copper zeolite, 80 mg for the iron zeolite) diluted with 60 mg of quartz powder were loaded in a flow-microreactor consisting of a quartz tube (6 mm i.d.) placed in an electric furnace. The catalyst powder was positioned between two layers of quartz wool, while corundum grains (average diameter = 1 mm) were used to fill the reactor to favour mixing of the gaseous species upstream from the catalyst powder.

He, NO_2, NH_3 and O_2 from calibrated mixtures with He in high pressure cylinders were dosed to the reactor by mass flow controllers (Brooks Instruments). The absence of traces of O_2 in the NO_2 bottles was guaranteed by the synthetic gas supplier. Argon was used as a tracer and internal standard for the analysis. All the lines upstream and downstream from the reactor were heated to 200 °C to prevent H_2O condensation, while the reaction temperature was monitored and controlled by a K-type thermocouple immersed in the catalyst bed.

Two four-port fast valves were used to perform stepwise switches between different gaseous feed streams: this assures that the overall flow rate remains constant, as an inert flow entering the reactor (He) is replaced by an equal flow containing the reactant (either NH_3 or NO_2). Furthermore, a backpressure regulator was positioned along the bypass line; in this way the backpressure of the bypass stream that has to be added to the reactor can be controlled in order to minimize pressure changes upon switching of the feed gases.

Care was taken also to avoid all possible dead volumes in the lines before and after the reactor. The overall dead time measured upon stepwise injection of an inert tracer (Ar) was in the order of 2 s, which is negligible with respect to the characteristic times of the measured responses, typically in the order of several minutes.

Downstream from the reactor the gas analysis section consisted of a quadrupole mass spectrometer (Balzers QMS 200) and of a UV analyzer (ABB–LIMAS 11 HW) arranged in a parallel configuration. The two instruments provided continuous measurement of N_2O and N_2, and of NH_3, NO, NO_2 concentrations, respectively, during the experiments.

Prior to the experimental campaign both catalysts were conditioned in a temperature ramp from r.t. up to 600 °C (5 °C/min) in 10% O_2 (v/v) + 10% H_2O (v/v), followed by hold at 600 °C for 5 h.

In a typical run, both step-response and temperature-programmed protocols were implemented. In the former case, step changes in the NO_2 feed concentration (0–1000–0 ppm) were realized by means of the four-way valve system described above while continuously feeding a dry helium stream to the reactor. The reactor temperature was meanwhile kept constant at either 120 °C or 200 °C.

After saturation of the catalyst with NO_2, a temperature-programmed experiment (heating rate = 20 °C/min, maximum temperature = 550 °C) was performed.

Prior to each test, the catalyst sample was pre-treated either in an oxidizing or reducing atmosphere. In the first case the catalyst was exposed to a helium stream containing 2% (v/v) of O_2. The treatment lasted 1 h at 550 °C, then the catalyst was cooled down to 200 °C, still under constant oxygen flow; the oxygen supply was eventually stopped only 30 min before exposing the catalyst to NO_2. The 550 °C temperature level was reached through a linear increase of the catalyst temperature in the presence of oxygen from about 40 °C. During this heat-up phase oxygen consumption with corresponding evolution of water was detected by the mass spectrometer for both the Fe-zeolite (Fig. 1A) and the Cu-zeolite (Fig. 1B): this indicates that both the catalysts were oxidized upon exposure to oxygen.

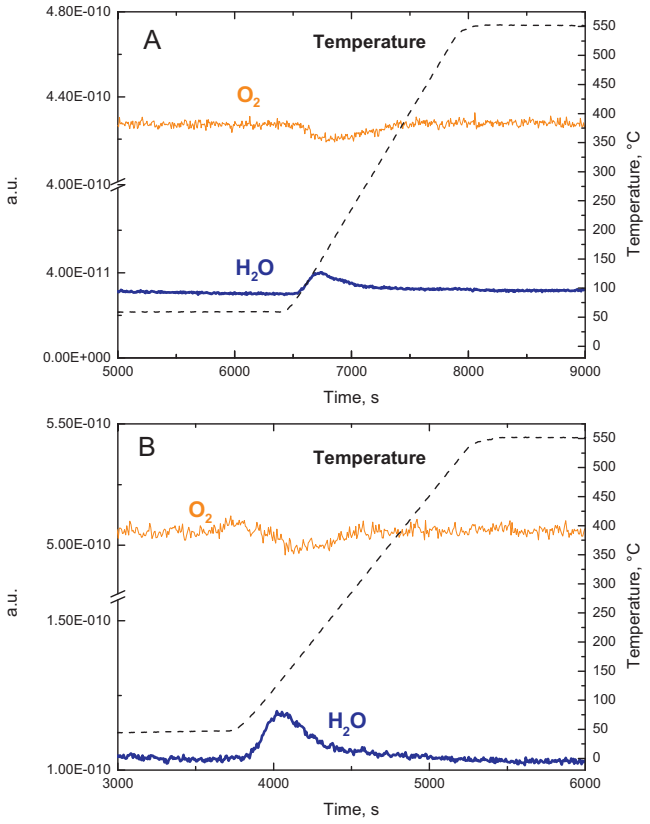

Fig. 1. Catalyst oxidation phase: Q = 71 cm^3/min (STP), O_2 = 2% (v/v), carrier gas = He, T-ramp = 20 °C/min. (A) Fe-zeolite (B) Cu-zeolite.

In the case of the reducing atmosphere, 1000 ppm of NH_3 were fed to the reactor at a constant temperature of 550 °C. As soon as ammonia was added to the feed stream, nitrogen was detected at the reactor outlet for both catalyst samples, indicating catalyst reduction by ammonia (Fig. 2). Over the Fe-zeolite sample a significant activity in the NH_3 decomposition to N_2 and H_2 was also observed (Fig. 2A), in line with literature indications [24,25]. On the contrary, in the case of the Cu-zeolite the nitrogen signal slowly dropped to zero, while the ammonia concentration eventually approached its feed value (Fig. 2B). After 1 h, ammonia was removed from the feed stream and the catalyst cooled down in a helium stream to 120 °C or 200 °C.

During all tests and pre-treatments, the system was operated at atmospheric pressure with gas hourly space velocities (GHSV) referred to the active phase of about 194,000 $cm^3/(h\,g_{cat})$ (STP) in the case of the Fe-zeolite catalyst, and 258,000 $cm^3/(h\,g_{cat})$ (STP) for the Cu-zeolite catalyst.

Further details on the experimental equipment and procedures can be found in Refs. [26–30].

3. Results and discussion

3.1. NO_2 adsorption/desorption on pre-oxidized Fe-zeolite

Figs. 3 and 4 show species outlet concentration traces obtained during typical two-stage runs performed over the tested Fe-zeolite catalyst. Prior to these experiments the catalyst was pre-treated in an oxidizing atmosphere, according to the procedure detailed

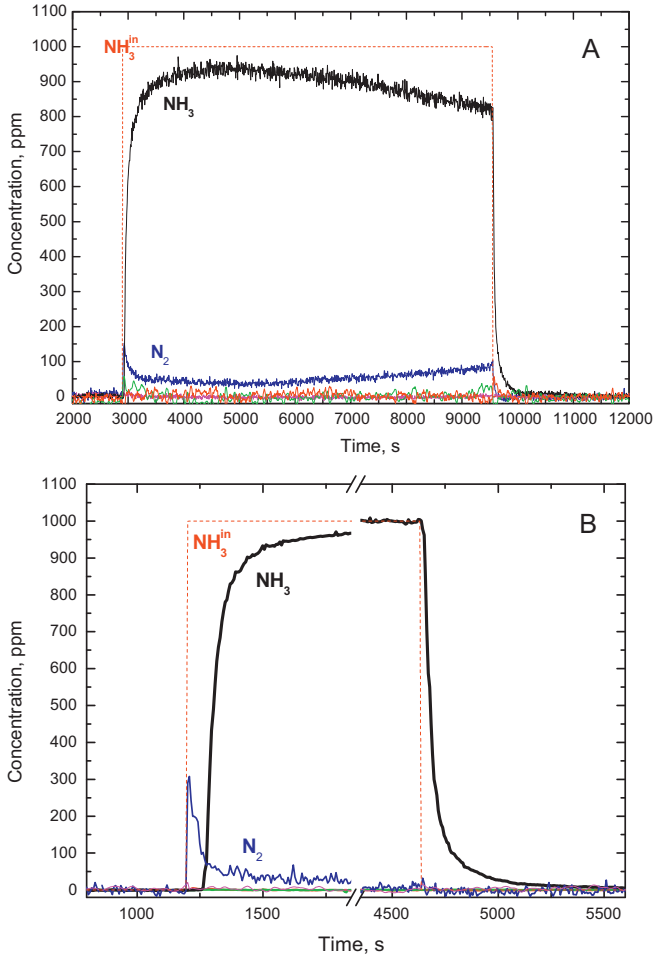

Fig. 2. Catalyst reduction phase: $Q = 71\ cm^3/min$ (STP), $NH_3 = 1000$ ppm, carrier gas = He, $T = 550\ ^\circ C$. (A) Fe-zeolite (B) Cu-zeolite.

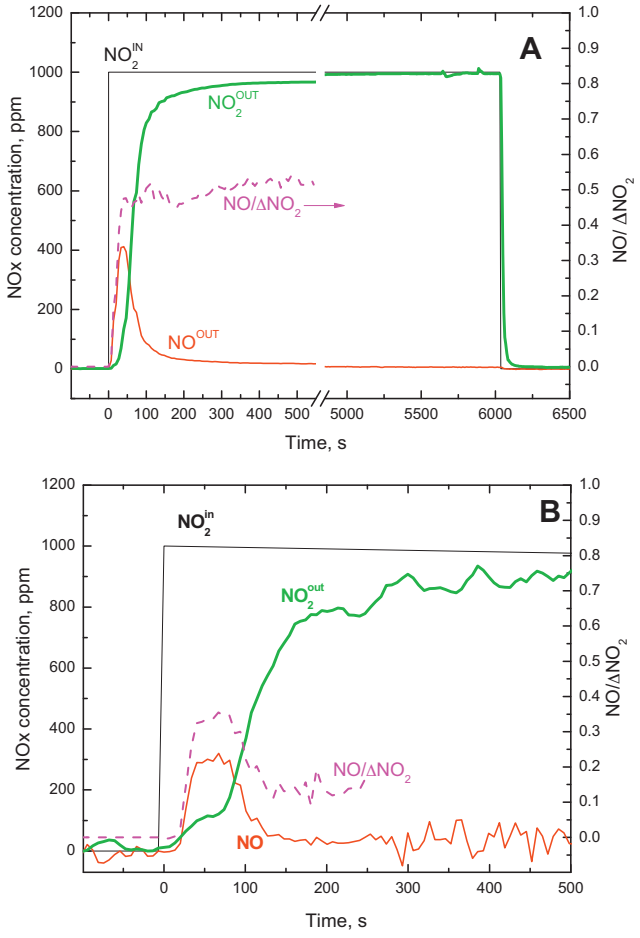

Fig. 3. Isothermal NO_2 adsorption over pre-oxidized Fe-zeolite: $Q = 71\ cm^3/min$ (STP), $NO_2 = 1000$ ppm, carrier gas = He; (A) $T = 200\ ^\circ C$, (B) $T = 120\ ^\circ C$.

in Section 2. Then, a step response experiment (Fig. 3) was first carried out feeding to the reactor 1000 ppm of NO_2 and balance helium either at 200 °C (Fig. 3A) or 120 °C (Fig. 3B). After approaching steady state conditions, the NO_2 feed was stopped, and finally the catalyst temperature was linearly increased at a constant rate of 20 °C/min up to 550 °C (Fig. 4A and B).

Inspection of Fig. 3A points out that, after NO_2 was fed to the reactor at $t = 0$ s, two distinct features were observed. First the NO_2 outlet concentration trace showed a dead time, followed by a rapid increase approaching the feed concentration. The second observed process was an immediate NO evolution as soon as NO_2 was fed to the reactor: the NO concentration reached a maximum of about 380–400 ppm and then dropped back to zero following a mirror image of the NO_2 trace. No other species, such as NH_3 or N_2O or N_2, were detected.

It has been widely reported in the literature [30–37] that zeolite catalysts are able to adsorb NO_2 at low temperatures in the form of nitrates. In the case of metal-promoted zeolites it is commonly recognized that the nitrates formation mainly occurs on metal sites [10,12–15,38], leading to the formation of relatively stable nitrates species, whose stability depends however on the metal involved. Formation of surface nitrate species upon NO_2 adsorption has been reported also for other materials such as alumina and titania [7–9].

The mechanism of NO_2 surface storage proposed by several authors can be described by the following two-step sequence, in which at first disproportionation of NO_2 to form surface nitrites and nitrates occurs (reaction (1)), followed by oxidation of nitrites by NO_2 to form more nitrates adspecies (reaction (2)):

$$2NO_2 + O^{2-} \leftrightarrow NO_3^- + NO_2^- \quad (1)$$

$$NO_2 + NO_2^- \leftrightarrow NO + NO_3^- \quad (2)$$

The same set of reactions was also proposed involving water, leading in this case to the formation of nitrous and nitric acid:

$$2NO_2 + H_2O \leftrightarrow HNO_3 + HNO_2 \quad (3)$$

$$NO_2 + HNO_2 \leftrightarrow NO + HNO_3 \quad (4)$$

Gaseous nitric acid could eventually adsorb onto the catalyst, thus explaining the storage of surface nitrates.

Another possible mechanism was proposed by England and Corcoran [39] for the gas phase reaction of water vapour and NO_2. According to these authors, after NO_2 disproportion and reaction with water, the formed nitrous acid would decompose to NO, NO_2 and water,

$$4NO_2 + 2H_2O \leftrightarrow 2HNO_3 + 2HNO_2 \quad (5)$$

$$2HNO_2 \leftrightarrow NO + NO_2 + H_2O \quad (6)$$

The same authors claimed that reaction (6) was much faster than reaction (4).

Remarkably, for all the proposed mechanisms the sum of the two considered steps (either reactions (1) + (2), or reactions (3) + (4), or

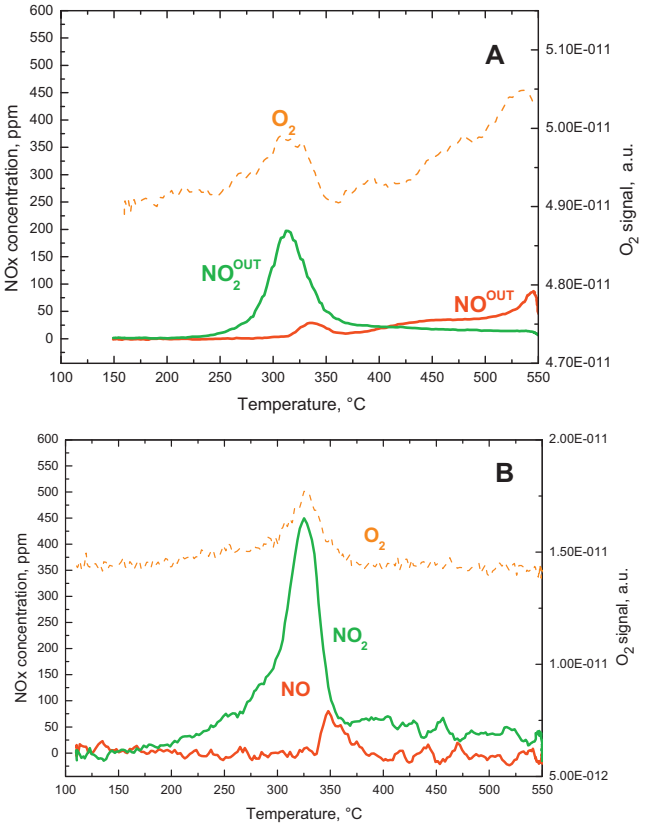

Fig. 4. NO_2 TPD over pre-oxidized Fe-zeolite: T-ramp = 20 °C/min, Q = 71 cm³/min (STP), He flow. (A) Adsorption phase at T = 200 °C; reactor filler: corundum grains (see Appendix A for more details). (B) Adsorption phase at T = 120 °C; reactor filler: quartz grains (see Appendix A for more details).

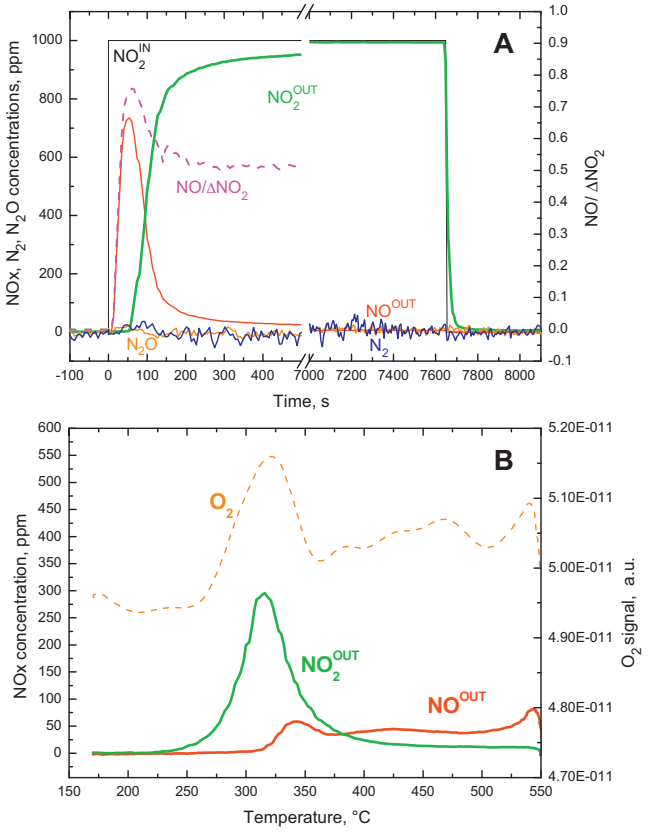

Fig. 5. NO_2 adsorption and TPD over pre-reduced Fe-zeolite: (A) isothermal adsorption/desorption: T = 200 °C, Q = 71 cm³/min (STP), NO_2 = 1000 ppm, carrier gas = He; (B) TPD run: T-ramp = 20 °C/min, Q = 71 cm³/min (STP), He flow.

reactions (5)+(6)) leads in any case to the following global stoichiometry,

$$3NO_2 + O^{2-} \leftrightarrow NO + 2NO_3^- \quad (7)$$

or, considering the presence of water,

$$3NO_2 + H_2O \leftrightarrow NO + 2HNO_3 \quad (8)$$

In both reactions (7) and (8) one mole of gaseous NO is produced for every three moles of adsorbed NO_2.

In Fig. 3A the molar ratio between produced NO and consumed NO_2 during the first 500 s of NO_2 feed is also plotted as a function of time. It can be noticed that during the initial NO evolution the ratio is close to 0.38–0.4, a value reasonably in agreement with the stoichiometry of reactions (7) and (8). After the catalyst reached steady state corresponding to catalyst saturation with nitrates, at t = 6000 s NO_2 was instantaneously removed from the feed flow, while continuously flowing He at the same constant temperature. It can be seen from Fig. 3A that, upon NO_2 shut-off, just a small NO_2 desorption tail was observed, indicating that at this temperature most of the nitrates formed on the catalyst surface were stable. This is also in line with FTIR data collected during NO_2 adsorption on different Fe-zeolites by several authors [3,13,40].

Fig. 3B shows the evolution of species outlet concentrations as well as the molar ratio between produced NO and consumed NO_2 during the initial NO_2 feed transient for a test carried out at 120 °C: in this case the ratio between produced NO and consumed NO_2 was 0.33, i.e. exactly in line with the expected stoichiometry of reactions (7) and (8). The following decrease of the $NO/\Delta NO_2$ ratio is likely related to the contribution of physisorbed NO_2, which cannot be ruled out at such low temperatures as 120 °C. Such a temperature effect led us to speculate that the slightly higher value recorded during the test at 200 °C was likely due to the partial decomposition of the formed nitrates, to give again NO_2, as discussed in the following. Accordingly, the mechanism of NO_2 adsorption represented by the overall stoichiometry of reactions (7) and (8) could be reasonably accepted also for the analysed iron zeolite catalyst pre-treated in an oxidizing atmosphere.

To confirm the presence of nitrates on the catalyst surface, and to study their thermal stability, a TPD run was performed following the isothermal adsorption/desorption phase. Fig. 4A shows the gas phase concentrations of NO and NO_2, plotted as a function of temperature, during the catalyst heat-up period following the adsorption phase at 200 °C. Evolution of NO_2 was evident above 230 °C, with a maximum of about 200 ppm centred around 320 °C. Above 300 °C also minor amounts of NO were detected. In correspondence of these desorption features oxygen was also detected, as shown by the MS signal in Fig. 4A. The time evolution of the species outlet concentrations were in line with the nitrates decomposition reaction:

$$2NO_3^- \rightarrow 2NO_2 + O^{2-} + 1/2O_2 \quad (9)$$

and the eventual decomposition of NO_2, controlled by the thermodynamic equilibrium of the reversible NO_2 decomposition reaction:

$$NO_2 \leftrightarrow NO + \tfrac{1}{2}O_2 \quad (10)$$

Notably, the results herein presented are consistent with what already observed for other zeolite systems [18,30,41], but also over $V_2O_5/WO_3/TiO_2$ catalysts [27].

Fig. 4A points out that desorption of NO/NO_2 continued above 370 °C, becoming again significant above 450 °C. However, this phenomenon is not related to desorption of nitrates from the tested zeolite catalyst (see Appendix A for more detailed information).

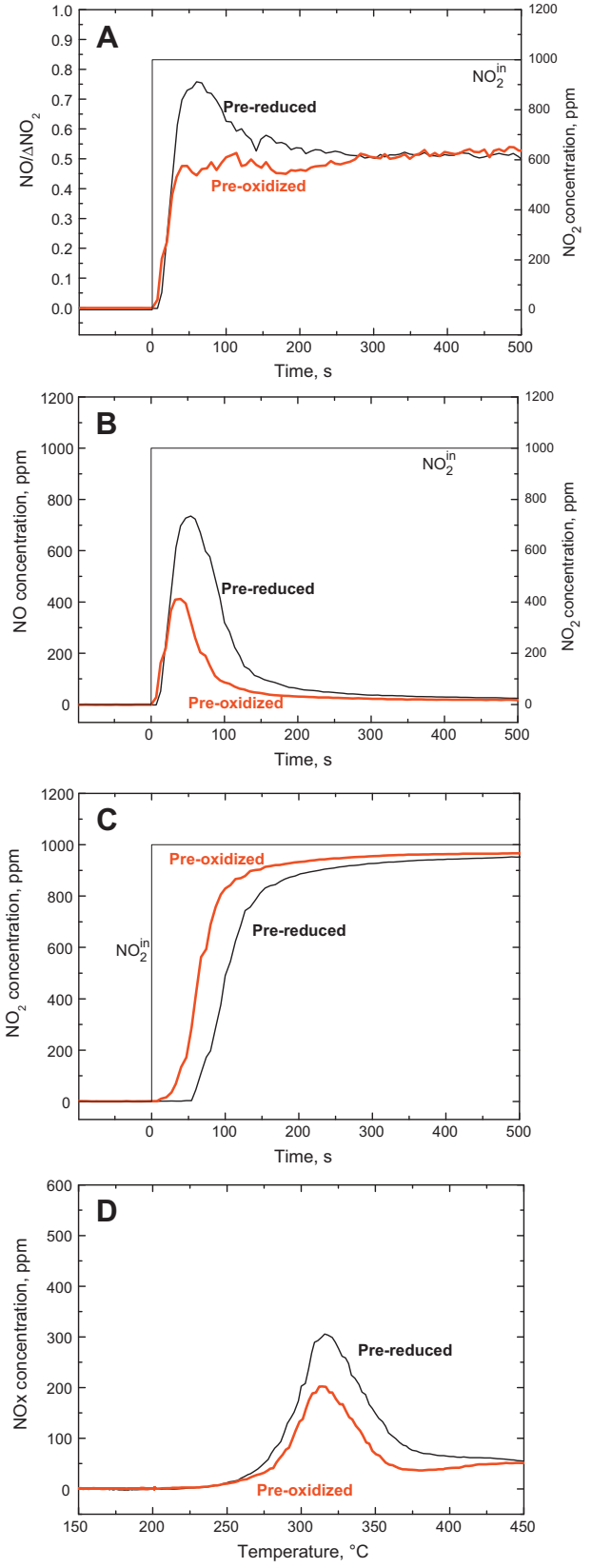

Fig. 6. Comparison of NO_2 adsorption and TPD over pre-oxidized and pre-reduced Fe-zeolite. Adsorption phase: T = 200 °C, Q = 71 cm³/min (STP), NO_2 = 1000 ppm, carrier gas = He. TPD: T-ramp = 20 °C/min, Q = 71 cm³/min (STP), He flow. (A) $NO/(NO_2^{in} - NO_2^{out})$ as a function of time during the first 500 s of NO_2 feed. (B) NO concentration as a function of time during the first 500 s of NO_2 feed. (C) NO_2 concentration as a function of time during the first 500 s of NO_2 feed. (D) NO_x concentration as a function of catalysts temperature during TPD phase. Black lines = pre-reduced sample. Red lines = pre-oxidized sample. (For interpretation of the references to color in this figure legend, the reader is referred to the web version of the article.)

A TPD test was also performed to study the thermal stability of nitrates stored on the catalyst surface at 120 °C. Results in Fig. 4B show evolution of NO_2 above 180 °C, with a maximum of about 460 ppm centred around 320 °C and minor amounts of NO detected above 300 °C. It is evident that these results are in good agreement with those discussed for Fig. 4A. Notably, it is worth underlying that the detected threshold temperature of NO_2 evolution was slightly below 200 °C: this information supports the fact that during the NO_2 adsorption phase of the run performed at 200 °C a part of the formed nitrates can indeed be decomposed back to NO_2, thus resulting in a molar ratio between produced NO and consumed NO_2 slightly higher than the theoretical value of 0.33 predicted by reactions (7) and (8).

3.2. *Effect of catalyst red–ox state on NO_2 adsorption/desorption on Fe-zeolite*

A step change plus TPD run, equal to the one described in the previous section, was carried out over the tested Fe-zeolite catalyst after pre-treating the sample in a reducing atmosphere according to the procedure described in Section 2. Thus, after exposure of the catalyst to ammonia at 550 °C, 1000 ppm of NO_2 and balance helium were fed to the reactor at 200 °C until steady state conditions were approached; the NO_2 feed was then stopped, and a temperature ramp at 20 °C/min was finally performed.

Results obtained during this test are reported in Fig. 5. The addition of NO_2 to the system resulted in a transient behaviour similar to that described in Section 3.1 over the pre-oxidized sample: NO evolution was immediately detected upon NO_2 feed, with this last species showing instead a dead time before its concentration increased and approached the feed level (Fig. 5A). No other species, such as NH_3 or N_2O or N_2, were detected (Fig. 5A), indicating that no NH_3 was left on the catalysts surface from the previous reducing pre-treatment. The following TPD phase resulted in the evolution of NO_2, NO and O_2, again qualitatively in line with what already discussed in Section 3.1.

Nonetheless, comparison of Figs. 3A, 4A and 5 points out significant quantitative differences between the samples pre-treated either in an oxidizing or in a reducing atmosphere. For this reason, results obtained during the test over the pre-reduced sample were comparatively analysed with those obtained over the catalyst pre-treated in an oxidizing atmosphere and presented in the previous section. The analysis was first focused on the species temporal evolution during the NO_2 adsorption period. Fig. 6A compares the $NO/\Delta NO_2$ molar ratios recorded during the first 500 s of NO_2 feed during both tests. A different behaviour in the first 300 s was clearly noted, the observed $NO/\Delta NO_2$ ratio being much higher over the catalyst previously exposed to a reducing atmosphere than over the oxidized system. In the case of the pre-reduced catalyst, the ratio increased as NO_2 was fed to the reactor, reached a maximum of about 0.75, and then recovered the same values of the pre-oxidized sample after 300 s.

Of course, the variation of the $NO/\Delta NO_2$ ratio corresponded to a different behaviour in the NO and NO_2 outlet traces, as apparent by inspection of Fig. 6B and C where the NO and NO_2 evolutions during the first 500 s of NO_2 feed are compared, respectively. In both tests, an immediate release of NO was recorded upon NO_2 feed and the qualitative behaviour of the NO trace was similar over the different pre-treated catalysts: after reaching a maximum value, the NO concentration dropped gradually to zero. However, in the

case of the sample pre-treated in a reducing atmosphere the maximum of the NO signal reached about 750 ppm, a value much higher than that obtained in the case of the pre-oxidized sample (about 400 ppm), and the integral amount of produced NO was also significantly greater. Correspondingly the dead-time observed in the NO_2 signal is greater in the case of the pre-reduced catalyst, being about 50 s against a value of about 15 s in the case of the sample pre-treated in oxidizing atmosphere.

A recent paper from Ahrens et al. has addressed the analysis of surface species evolution during both NO_2 and NO adsorption over two different Fe-zeolite catalysts [3]. The in situ FTIR analysis therein reported was conducted after activating the samples under two different conditions, in order to control the oxidation state of Fe. Ahrens et al. found that, upon addition of NO_2, only a small increase in the band related to Fe^{3+}–OH groups was observed for the oxygen-treated sample, while a significant increase of the intensity of the same band was detected for the sample activate under vacuum conditions (reducing treatment). Such Fe^{3+}–OH groups were then consumed upon continuing the adsorption process, leading to the formation of ferric nitrate species.

The initial increase of such a band was justified by the authors considering that, after the vacuum pre-treatment, a higher amount of Fe^{2+} species were present. The addition of NO_2, a strong oxidizing agent, caused then the following reaction:

$$2Z\text{–}Fe^{2+} + NO_2 \rightarrow Z\text{–}Fe^{3+}\text{–}O^- + Z\text{–}Fe^{2+}\text{–}NO \quad (11)$$

were NO_2 oxidizes the Fe^{2+} species, with a simultaneous production of NO, temporarily adsorbed over other remaining reduced Fe^{2+} sites in the form of nitrosyl adspecies.

The same authors also pointed out another significant difference between the dynamic behaviours of their Fe-zeolite samples activated under either vacuum or oxygen atmospheres. Indeed, over both samples a band around 1880 cm^{-1}, assigned to the formation of nitrosyl Fe^{2+}–NO species, appeared and increased upon addition of NO_2, but then decreased and finally vanished with further equilibrium NO_2 pressure. However, the band maximum intensity was found to be four times higher for the vacuum-activated sample than for the oxygen activated one. The authors explained these deviations with the presence of a much greater amount of Fe^{2+} cations in the case of the vacuum activated sample.

It is worth mentioning however that the assignment of the band around 1880 cm^{-1} is controversial in the literature: although the band is commonly assigned to nitrosyl species on Fe sites, different oxidation state are attributed to the Fe: Segawa et al. [42] and Rivallan et al. [17] assigned the band to Fe^{3+}–NO species, while Ahrens et al. [3], Hadjiivanov et al. [43], Kefirov et al. [44] and Mul et al. [45] assigned the band to Fe^{2+}–NO species.

As shown in Figs. 3A and 4A, and discussed in the previous paragraph, the analysis of gas phase species evolution during NO_2 adsorption pointed out that, for a catalyst pre-treated in an oxidizing atmosphere, a $NO/\Delta NO_2$ ratio close to 1/3 was achieved, in line with the well-known two step NO_2 adsorption mechanism previously discussed, which does not involve changes in the catalyst oxidation state. On the other hand, for a catalyst pre-treated in reducing atmosphere a significantly higher evolution of NO during the initial transient, and correspondingly a higher $NO/\Delta NO_2$ molar ratio, were measured, as already discussed and shown in Fig. 6A and B. Coupling these results with those from Ahrens et al. [3], we can sketch the following picture for NO_2 adsorption over a catalyst pre-exposed to a reducing atmosphere: Fe^{2+} species, initially abundant on the catalyst surface after the reducing pre-treatment, are first oxidized by NO_2 according to the following global reaction:

$$2Z\text{–}Fe^{2+} + NO_2 + H_2O \rightarrow 2Z\text{–}Fe^{3+}\text{–}OH + NO \quad (12)$$

This reaction leads to the formation of Fe^{3+}–OH species, where the classical two step NO_2 adsorption mechanism can then take place according to the global reaction:

$$2Z\text{–}Fe^{3+}\text{–}OH + 3NO_2 \rightarrow 2Z\text{–}Fe^{3+}\text{–}NO_3 + NO \quad (13)$$

Furthermore, catalyst re-oxidation involves the formation of one mole of NO for every mole of converted NO_2, thus leading to higher NO evolution and higher $NO/\Delta NO_2$ ratios compared to a pre-oxidized catalyst, where the stoichiometry is controlled by reaction (13). Consequently, the more abundant formation of NO during the initial transient of NO_2 adsorption justifies the increased intensity of the iron nitrosyl band around 1880 cm^{-1} observed by Ahrens et al. [3] over the vacuum activated sample, regardless of its assignment to Fe^{2+}–NO or Fe^{3+}–NO species.

Another work focusing on NO evolution during NO_2 adsorption on a Fe-ZSM-5 catalyst was recently published by Iwasaki and Shinjoh [10]. The authors analysed the evolution of both gas phase and surface species over a catalyst pre-treated in oxygen at high temperature. Experimental results from the gas phase, obtained in the absence of water, suggested a stoichiometry in line with reaction (7) for NO_2 adsorption over Fe species. However, the authors proposed a new mechanism for NO_2 adsorption: the scheme involves first the decomposition of NO_2 over Fe binuclear sites to give NO and bridging oxygen, with NO temporarily adsorbed onto the Fe sites; then follow-on NO_2 replaced adsorbed NO, thus evolving in the gas phase. The adsorption of one molecule of NO_2 for every Fe site gives, for every binuclear site, a stoichiometry of one mole of NO produced every 3 moles of consumed NO_2. Such a stoichiometry is consistent with the pre-treatment of the catalyst in an oxidizing atmosphere, according to the results presented in this work. However, the oxidation state of Fe binuclear species in such a scheme was not fully clarified by the authors, and the increased amount of NO released from a catalyst pre-treated in a reducing atmosphere emphasized by the present work can hardly be justified by such a scheme.

After analyzing the effect of the catalyst pre-treatment on the dynamics of NO_2 adsorption, the subsequent NO_x evolution during the temperature programmed desorption phase of the two tests is also compared in Fig. 6D, reporting the NO_x outlet concentration as a function of temperature. The figure shows that the shape of the desorption peaks recorded during the two tests over the pre-oxidized and over the pre-reduced sample were qualitatively similar, both being centred around 320 °C; however, a significantly greater amount of NO_x was released in the case of the catalyst pre-treated in a reducing atmosphere. The same qualitative result was also reported by Ahrens et al. [3]: after sample activation in vacuum, the bands related to the iron-nitrates were found to be more intense compared to what was observed over the sample pre-treated under oxidizing conditions. Based on NO adsorption, H_2-TPR and FTIR measurements, it has been proposed in the literature that CO reduction can result in what seems to be a re-dispersion of the Fe in Fe-ZSM-5 catalysts, thus providing additional Fe^{2+} sites at the expenses of FeO_x species [46]. In the cited paper six Fe-ZSM-5 zeolites with different Fe loadings were tested in the NO adsorption at room temperature and H_2-TPR after different pre-treatments, either in oxidizing or reducing atmosphere. The paper clearly demonstrates that the oxidation state of Fe species was a function both of the pre-treatment and of the Fe content. The authors proved that for Fe/Al above 0.56 FeO_x particles are formed in the zeolite; such particles can then be reduced by CO, with the subsequent dispersion of Fe as Fe^{2+} cations, thus forming additional sites for NO adsorption at room temperature. Generalizing the literature findings we can speculate that the Fe re-dispersion occurred also over our tested zeolite sample upon exposure to NH_3

as a reducing agent, thus resulting in the presence of additional Fe sites for nitrates storage.

The effect of catalyst pre-treatment was also analysed in the case of NO_2 adsorption at 120 °C. Fig. 7 compares experimental results collected after the oxidizing and the reducing pre-treatments. Fig. 7A shows $NO/\Delta NO_2$ molar ratios close to 0.33 for both pre-treatments in the first seconds after NO_2 feed to the catalyst. A slightly higher value was recorded in the case of the reducing pre-treatment. Consistently with the picture previously proposed for the NO_2 interaction with a pre-reduced sample, we can speculate that the decrease of the adsorption temperature resulted in a slower rate of catalyst re-oxidation, thus leading to NO/NO_2 ratios not significantly higher than 0.33 also in the case of the pre-reduced sample. Clear differences are instead evident in terms of NO and NO_2 concentration profiles during the NO_2 feed transient depending on the catalyst pre-treatment: greater evolution of NO and longer dead time before NO_2 breakthrough were recorded over the sample pre-treated in a reducing atmosphere, likely indicating the formation of a higher amount of stored nitrates. This was confirmed by the subsequent TPD, where the amount of NO_x desorbed from the pre-reduced sample was greater than that recorded for the pre-oxidized one. The effect of catalyst pre-treatment on nitrates storage capacity was completely in line with that discussed for the adsorption test carried out at 200 °C.

3.3. *Effect of catalyst red–ox state on NO_2 adsorption/desorption on Cu-zeolite*

After the Fe-zeolite catalyst, a Cu-metal promoted zeolite system was considered, as well. Step response + TPD experiments, equal to those described in the previous sections for the Fe-zeolite, were carried out over the tested Cu-zeolite catalyst after pretreating the sample either under oxidizing or reducing atmosphere, according to the procedures detailed in Section 2. Once again, after either the oxidizing or the reducing pre-treatment, the catalyst was exposed to a gaseous stream containing 1000 ppm of NO_2 in helium at a constant temperature of 200 °C; once steady state conditions were approached the NO_2 feed was then stopped and a temperature ramp at 20 °C/min was performed.

Results obtained during these tests were then comparatively analysed in terms of $NO/\Delta NO_2$ ratio, NO and NO_2 evolution during the NO_2 adsorption dynamics as well as in terms of NO_x desorption during the temperature ramp.

Fig. 8A shows the $NO/\Delta NO_2$ molar ratio measured over the Cu-zeolite during the first 500 s of NO_2 feed in the runs over the pre-reduced and over the pre-oxidized sample. Similar to what observed in the case of the Fe-zeolite (see Fig. 6A), the $NO/\Delta NO_2$ ratio was consistently higher over the catalyst pre-exposed to a reducing atmosphere. Correspondingly, Fig. 8B, shows that a higher concentration of NO was recorded in the case of the pre-reduced sample, again in line with the results over Fe-zeolite catalyst. Furthermore, the analysis of the NO_2 evolution (Fig. 8C) highlighted a longer dead-time before breakthrough over the pre-reduced sample, estimated in 80 s in the case of the pre-reduced sample against 35 s for the pre-oxidized one. However, the increment in the NO evolution associated with the reducing pretreatment was significantly less marked over the Cu-zeolite than over the Fe-zeolite.

As discussed in the previous paragraph, we attributed the higher NO evolution during the first seconds of NO_2 adsorption onto the pre-reduced Fe-zeolite to catalyst oxidation by NO_2. The same mechanism can be assumed also to justify the greater NO evolution observed in the case of the Cu-zeolite sample pre-treated in a reducing atmosphere. The fact that in this case the deviation between the results over pre-reduced and pre-oxidized samples was less pronounced compared to that over the Fe-zeolite catalyst could be due to different reasons. First, we can speculate that, under the adopted

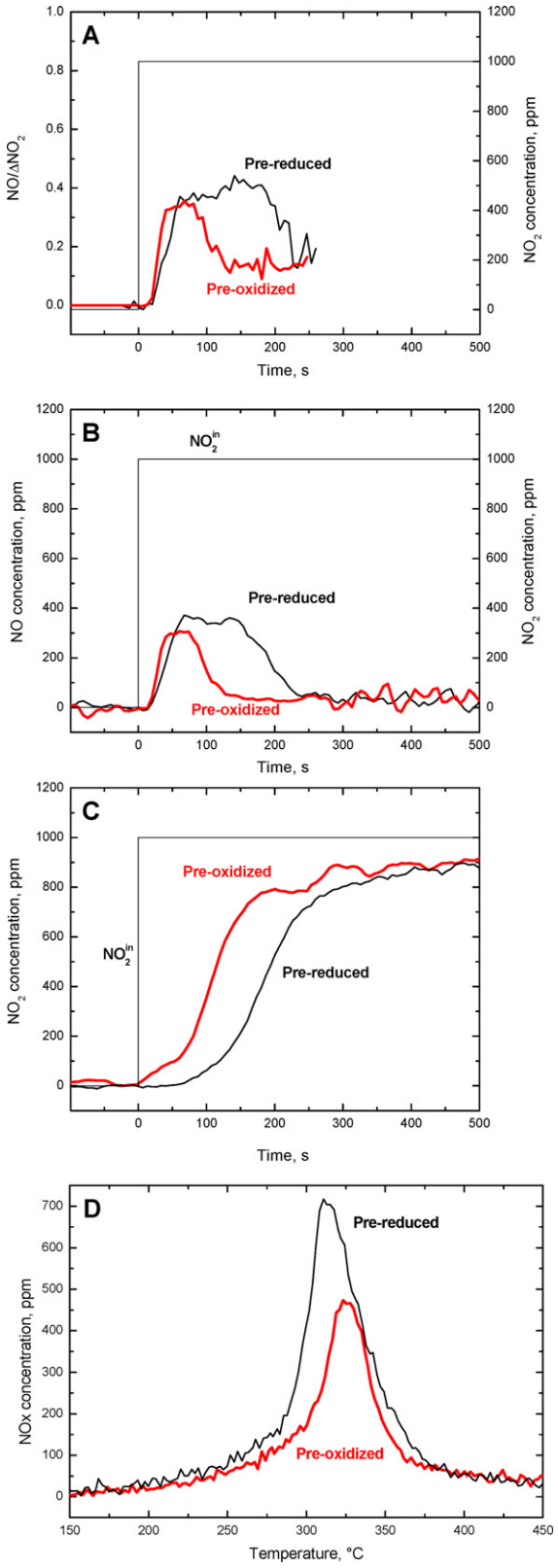

Fig. 7. Comparison of NO_2 adsorption and TPD over pre-oxidized and pre-reduced Fe-zeolite. Adsorption phase: T = 120 °C, Q = 71 cm³/min (STP), NO_2 = 1000 ppm, carrier gas = He. TPD: T-ramp = 20 °C/min, Q = 71 cm³/min (STP), He flow. (A) $NO/(NO_2^{in} - NO_2^{out})$ as a function of time during the first 500 s of NO_2 feed. (B) NO concentration as a function of time during the first 500 s of NO_2 feed. (C) NO_2 concentration as a function of time during the first 500 s of NO_2 feed. (D) NO_x concentration as a function of catalysts temperature during TPD phase. Black lines = pre-reduced sample. Red lines = pre-oxidized sample. (For interpretation of the references to color in this figure legend, the reader is referred to the web version of the article.)

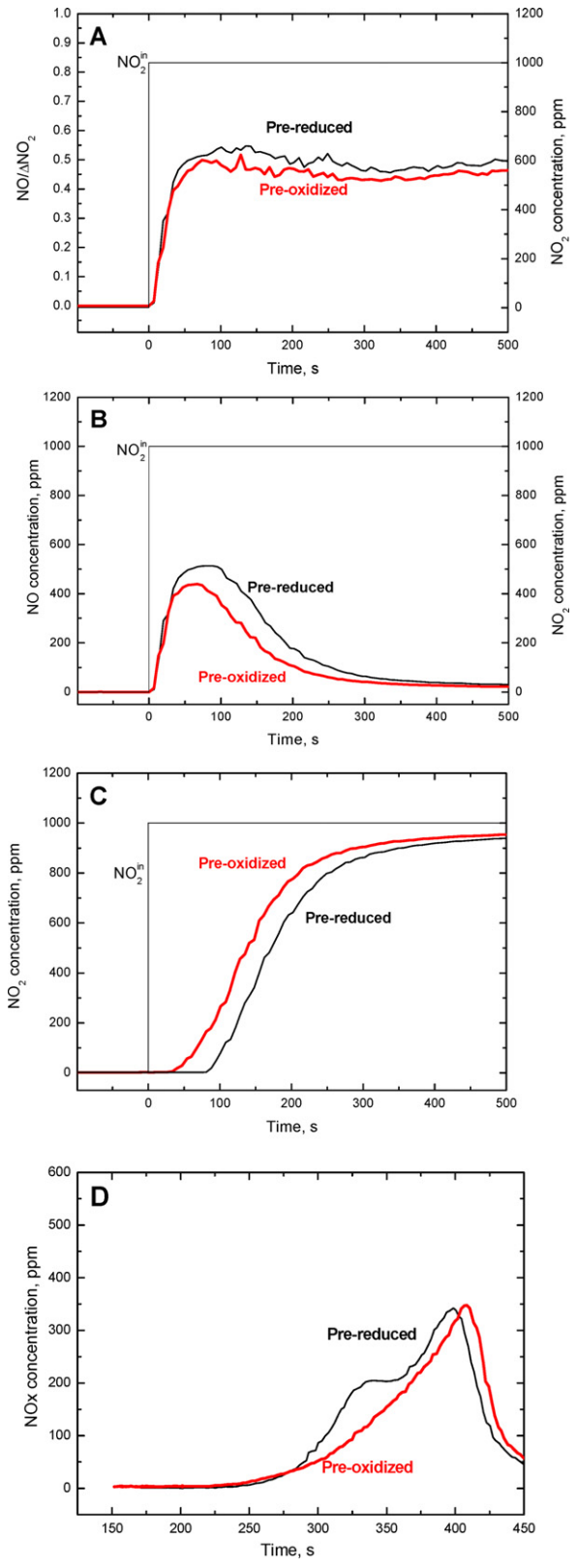

Fig. 8. Comparison of NO_2 adsorption and TPD over pre-oxidized and pre-reduced Cu-zeolite. Adsorption phase: T = 200 °C, Q = 71 cm³/min (STP), NO_2 = 1000 ppm, carrier gas = He; TPD: T-ramp = 20 °C/min, Q = 71 cm³/min (STP), He flow. (A) $NO/(NO_2^{in} - NO_2^{out})$ as a function of time during the first 500 s of NO_2 feed. (B) NO concentration as a function of time during the first 500 s of NO_2 feed. (C) NO_2 concentration as a function of time during the first 500 s of NO_2 feed. (D) NO_x concentration as a function of catalysts temperature during TPD phase. Black lines = pre-reduced sample. Red lines = pre-oxidized sample. (For interpretation of the references to color in this figure legend, the reader is referred to the web version of the article.)

experimental conditions, the oxidation of Cu reduced species by NO_2 is slower than that of Fe^{2+} species. Another explanation for the smaller deviations in the case of the Cu-zeolite catalyst could be related to the experimental procedure adopted for the oxidizing pre-treatment. As described in Section 2, the oxidation procedure consisted in exposing the catalyst to oxygen at high temperatures, followed by cool down. Once reached the adsorption temperature of 200 °C, the oxygen supply was stopped and for a certain period of time, prior to NO_2 feed, the catalyst was exposed to helium flow, i.e. to an inert atmosphere. In these conditions we cannot rule out that a partial auto-reduction of the catalyst occurred, as already reported in the literature [47,48]. In order to prevent any change in the catalyst oxidation state after the oxidizing pre-treatment, NO_2 adsorption tests were replicated in the presence of oxygen over both the Fe- and the Cu-zeolite catalyst. Results are presented and discussed in the following section.

Fig. 8D shows the NO_x outlet concentrations versus the catalyst temperature during the temperature programmed desorption run performed over both the pre-reduced and the pre-oxidized Cu-zeolite catalyst after NO_2 saturation. In the case of the catalyst pre-exposed to an oxidizing atmosphere, a broad desorption peak, centred at about 400 °C can be noticed. However, the asymmetry of the desorption peak, with a significant tail between 250 °C and 350 °C, suggests the existence of multiple adsorption sites. In the case of the catalyst pre-treated in a reducing atmosphere, the NO_x desorption profile shows the existence of an additional peak, centred at 320 °C, besides the one observed also over the pre-oxidized sample. In analogy with the Fe-zeolite sample, we speculate that also for the Cu-zeolite catalyst the pre-treatment in a reducing atmosphere resulted in the re-dispersion of part of the Cu in the zeolite. Furthermore it is also well established in the literature that different Cu ions with different reducibility and oxidation activity can be present in Cu-promoted zeolites [49,50], thus resulting in the presence of different nitrate species on the catalyst surface characterized by different thermal stabilities.

3.4. NO_2 adsorption/desorption on Fe- and Cu-zeolite in the presence of gaseous oxygen

As discussed in the previous section, the effect of catalyst pre-treatment either in an oxidizing or reducing atmosphere was found to be less pronounced over the tested Cu-zeolite catalyst. However, the oxidizing procedure defined in Section 2 involved catalyst exposure to an inert atmosphere, though to a limited time extent, being the catalyst flushed with just helium at 200 °C prior to NO_2 adsorption. In order to clarify if this could have altered the catalyst oxidation state, NO_2 adsorption tests over both Fe- and Cu-zeolites were replicated according to the following procedure: the catalyst was first exposed for 1 h to a stream containing 2% (v/v) O_2 at a constant temperature of 550 °C, then the catalyst was cooled down to 200 °C. Still keeping a constant oxygen feed, 1000 ppm of NO_2 were stepwise fed to the reactor until steady state. First NO_2 and a few minutes later O_2 were then removed from the feed stream and the catalyst temperature was finally increased at a constant rate of 20 °C/min up to 550 °C.

Results obtained during these experiments were then comparatively analysed with those collected over both catalysts after the standard reducing or oxidizing protocols.

Fig. 9A–C shows experimental results over the Fe-zeolite in terms of $NO/\Delta NO_2$ ratio, NO and NO_2 concentration respectively during the first seconds after the NO_2 feed. The data for pre-oxidized and pre-reduced catalysts are the same presented in Fig. 6, while the green, thick lines represent experimental data recorded in the continuous presence of oxygen. It clearly appears that these last results, collected by cofeeding NO_2 and oxygen, are very similar to those obtained over the pre-oxidized sample. We can thus

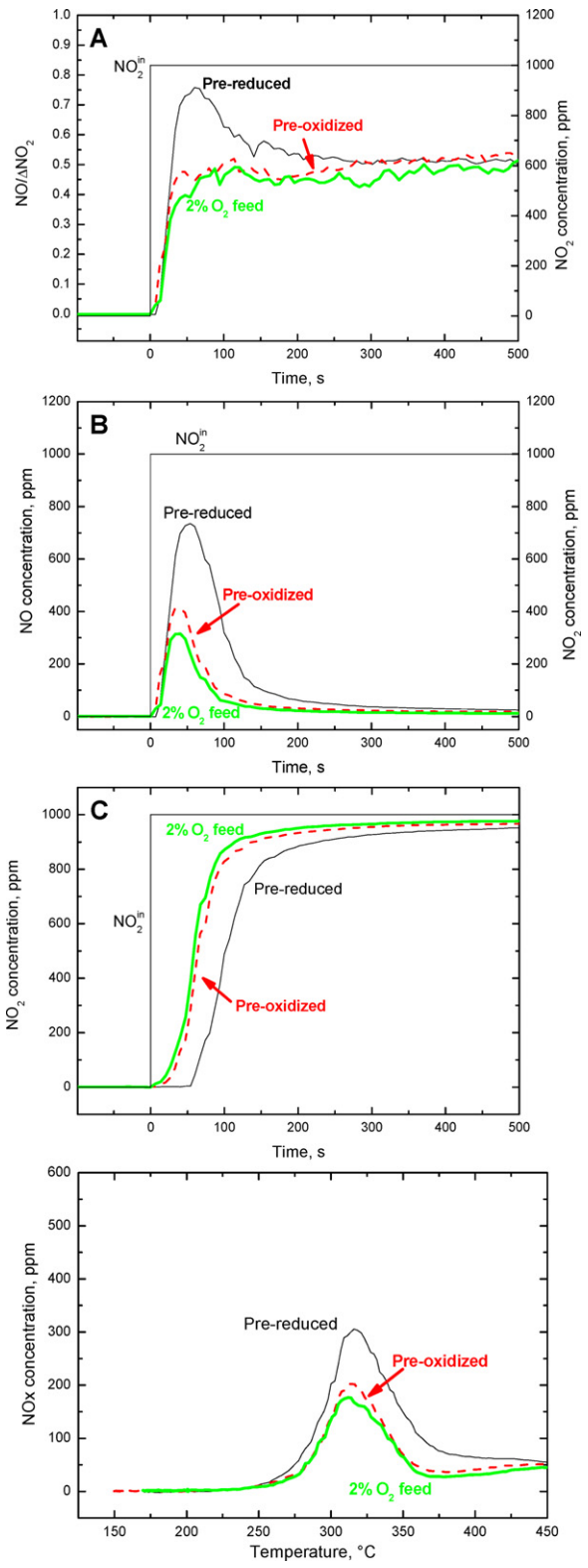

Fig. 9. NO_2 adsorption and TPD over Fe-zeolite. Adsorption phase: $T = 200\,^{\circ}C$, $Q = 71\,cm^3/min$ (STP), $NO_2 = 1000\,ppm$, $O_2 = 2\%$ (v/v) (only for green lines), carrier gas = He; TPD: T-ramp = 20 °C/min, $Q = 71\,cm^3/min$ (STP), He flow. A) $NO/(NO_2^{in} - NO_2^{out})$ as a function of time during the first 500 s of NO_2 feed. (B) NO concentration as a function of time during the first 500 s of NO_2 feed. (C) NO_2 concentration as a function of time during the first 500 s of NO_2 feed. (D) NO_x concentration as a function of catalysts temperature during TPD phase. Black lines = pre-reduced sample. Red lines = pre-oxidized sample. Green lines = pre-oxidized sample in the presence of oxygen during adsorption phase. (For interpretation of the references to color in this figure legend, the reader is referred to the web version of the article.)

conclude that the implemented oxidation procedure was fully effective over the tested iron zeolite catalyst, and that the exposure of the catalyst to He at 200 °C for a limited period of time did not affect the catalyst red–ox state.

A different situation was noted in the case of the Cu-zeolite catalyst: Fig. 10A–D again shows the data collected during NO_2 adsorption in terms of $NO/\Delta NO_2$ (Fig. 10A) ratio, NO and NO_2 concentrations (Fig. 10B and C, respectively) over the pre-reduced, the pre-oxidized catalysts and in the case of NO_2 pulse in co-presence of oxygen, and the subsequent TPD runs (Fig. 10D).

A significant effect of the oxygen presence on the NO_2 adsorption dynamics is apparent from inspection of Fig. 10. Indeed, when oxygen was present in the feed stream together with NO_2, a lower amount of NO was produced upon NO_2 step feed with respect to what observed over both the pre-oxidized and the pre-reduced samples. A $NO/\Delta NO_2$ ratio of about 0.35–0.38 was consistently recorded, in line with the stoichiometry of reactions (7)–(8). These data, according also to our interpretation of the results collected over the tested Fe-zeolite catalyst, are in line with those expected from an oxidized catalyst. Accordingly, we can speculate that the implemented oxidizing procedure was not completely effective over the tested Cu-zeolite sample. Indeed the analysis of the data in Fig. 10 indicates that at least a partial reduction of the Cu sites took place before NO_2 adsorption, during the implementation of the oxidation protocol, thus leading to $NO/\Delta NO_2$ ratios higher than expected from a fully oxidized sample, and as consistently recorded in the presence of oxygen. According to the adopted experimental procedure, in fact, the catalyst, prior to NO_2 adsorption, was exposed to a non-oxidizing atmosphere at 200 °C, when it was flushed with helium only. We can thus assume that, in the case of the tested Cu-zeolite a partial reduction of the catalytic surface occurred at 200 °C during the catalyst exposure to an inert atmosphere. This was not observed in the case of the Fe-zeolite, thus suggesting a greater reducibility of the Cu catalyst.

After removal of NO_2 and oxygen from the gas phase, a temperature ramp was performed, leading to desorption of previously adsorbed nitrates with evolution of NO_x. From Figs. 9D and 10D it appears that, in the case of both Fe- and Cu- zeolites, the NO_x desorption trace obtained after NO_2 adsorption in the presence of gaseous oxygen was identical to that obtained over the sample pretreated in an oxidizing atmosphere. From the TPD results it can thus be speculated that O_2 presence during adsorption of NO_2 did not affect the stability of the formed adspecies.

3.5. Quantitative analysis

A quantitative analysis was carried out in order to support the proposed scheme for NO_2 adsorption on the pre-reduced Fe- and Cu-zeolite catalyst samples. Table 1 and Table 2 show, for the Fe- and for the Cu-zeolite respectively, the integral amounts of stored

Table 1
Stored nitrates and produced NO over the Fe-zeolite sample.

	Adsorbed nitrates [mmol]	Produced NO [mmol]
NO_2 adsorption in presence of O_2	2.058E−3	1.030E−3
Pre-reduced sample	3.577E−3	3.476E−3

Table 2
Stored nitrates and produced NO over the Cu-zeolite sample.

	Adsorbed nitrates [mmol]	Produced NO [mmol]
NO_2 adsorption in presence of O_2	4.460E−3	2.230E−3
Pre-reduced sample	4.834E−3	4.380E−3

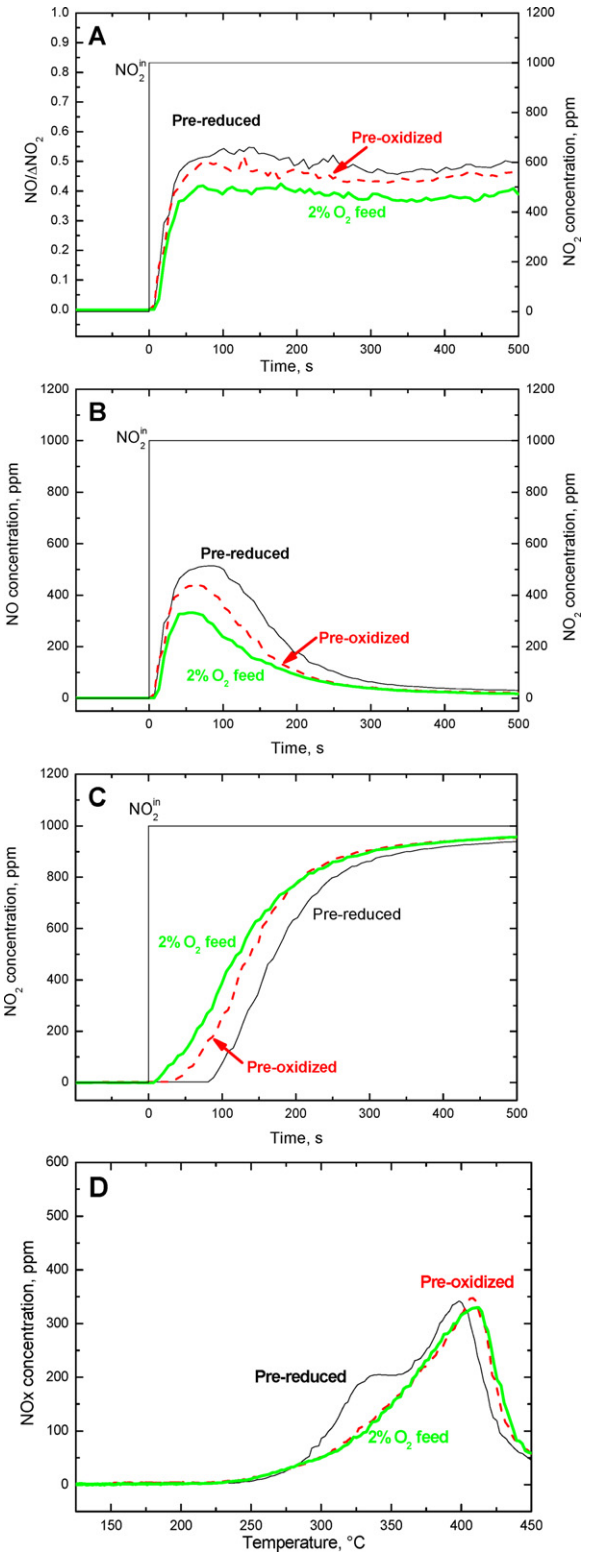

Fig. 10. NO_2 adsorption and TPD over Cu-zeolite. Adsorption phase: T = 200 °C, Q = 71 cm^3/min (STP), NO_2 = 1000 ppm, O_2 = 2% (v/v) (only for green lines), carrier gas = He; TPD: T-ramp = 20 °C/min, Q = 71 cm^3/min (STP), He flow. (A) $NO/(NO_2^{in} - NO_2^{out})$ as a function of time during the first 500 s of NO_2 feed. (B) NO concentration as a function of time during the first 500 s of NO_2 feed. (C) NO_2 concentration as a function of time during the first 500 s of NO_2 feed. (D) NO_x concentration as a function of catalysts temperature during TPD phase. Black lines = pre-reduced sample. Red lines = pre-oxidized sample. Green lines = pre-oxidized sample in the presence of oxygen during adsorption phase. (For interpretation of the references to color in this figure legend, the reader is referred to the web version of the article.)

nitrates calculated both for the tests carried out in the presence of gaseous oxygen and in the case of the reductive pre-treatment. These values were calculated integrating in time the NO and NO_2 concentration traces during the TPD phase up to 450 °C: in this way only the storage of nitrates on the catalyst surface was considered, avoiding spurious contributions (see Appendix A for more details). Table 1 and Table 2 report also the integral amounts of NO released during the NO_2 feed transients. Starting from the Fe-zeolite sample and according to the stoichiometry of reactions (12) and (13), the amount of Fe^{2+} ions present at the catalyst surface after the reductive pre-treatment should equal the difference between the amount of NO produced over the pre-reduced sample and over the sample exposed to NO_2–O_2. However, a greater amount of nitrates was stored in the case of the pre-reduced sample, thus the additional formation of NO related to the higher storage capacity should be considered. Assuming that the additional nitrates storage occurs via the disproportionation mechanism (13), one mole of NO is produced every two moles of stored nitrates. For this reason, the amount of additional NO related to the higher nitrates storage can be calculated dividing by two the difference between the amounts of nitrates stored on the pre-reduced and on the NO_2/O_2 exposed sample:

Additional NO = ½ × (NO_2 storage on pre-reduced sample – NO_2 storage on NO_2/O_2 exposed sample) = 7.595E−4 mmol.

The amount of Fe^{2+} ions resulted thus to be:

Amount of Fe^{+2} = 2 × (NO from pre-reduced sample – NO from NO_2/O_2 exposed sample – Additional NO) = 3.376E−3 mmol.

The amount of Fe^{2+} can also be directly calculated from the amount of stored nitrates or of produced NO in the case of the pre-reduced sample. Indeed, the sum of reactions (12) and (13) is:

$$2Z\text{–}Fe^{2+} + 4NO_2 \rightarrow 2Z\text{–}Fe^{3+}\text{–}NO_3 + 2NO \quad (14)$$

The amounts of stored nitrates and produced NO in the case of the pre-reduced sample are reported in Table 1 and are in good agreement with the previously calculated value. Furthermore, the amount of Fe sites involved in the storage of nitrates resulted to be lower by an order of magnitude with respect to the total amount of Fe in the tested zeolite.

In the case of the Cu-zeolite the following reactions can be proposed, in analogy to what assumed for the Fe-zeolite:

$$2Z\text{–}Cu^{+} + NO_2 + H_2O \rightarrow 2Z\text{–}Cu^{2+}\text{–}OH + NO \quad (15)$$

$$Z\text{–}Cu^{2+}\text{–}OH + 3NO_2 \rightarrow 2Z\text{–}Cu^{2+}\text{–}NO_3 + NO \quad (16)$$

The presence of Cu^{2+}–OH species has been also previously reported in the literature [47].

Applying the same methodology discussed for the Fe-zeolite, the following results are computed:

Additional NO = ½ × (NO_2 storage on pre-reduced – NO_2 storage on pre-oxidized) = 1.872E−4 mmol.

Amount of Cu^{+} = 2 × (NO from pre-reduced – NO from pre-oxidized – Additional NO) = 3.926E−3 mmol.

This value resulted to be lower than that based on stored nitrates and produced NO in the case of the pre-reduced sample (see Table 2). However the difference between these values can be considered of the same order of magnitude of the experimental error in computing the integral amounts.

The amount of Cu+ calculated according to the proposed scheme was finally compared with the total amount of Cu in the tested sample, and resulted to be of the same order of magnitude, thus indicating that for the tested Cu zeolite almost the entire amount of Cu was involved in the storage of nitrates.

4. Conclusions

We have presented a dedicated study of the interaction between NO_2 and two different metal promoted zeolite SCR catalysts wherein we analyse the species evolution depending on the initial catalyst red–ox state, a topic not clearly addressed and often overlooked in previous literature.

Experiments were carried out with dry feeds over both a Fe- and a Cu- zeolite commercial catalyst, involving first the adsorption of NO_2 at 200 °C, then the temperature programmed desorption of the formed adspecies. Prior to each experiment, the catalyst red–ox state was controlled by performing a treatment either in an oxidizing or in a reducing atmosphere. Additional experiments were also carried out in the presence of gaseous oxygen during the NO_2 adsorption phase.

Upon exposure to NO_2, formation of stable surface nitrates occurs over both the Fe- and the Cu-zeolite, as confirmed by the TPD results. However for both catalytic systems the dynamics of NO_2 adsorption and nitrates formation were substantially influenced by the initial catalyst red–ox state. Indeed, in all cases evolution of NO in the gas phase was recorded in the first minutes after NO_2 feed, but the concentration and the overall released amount of this species were greatly different depending on the catalyst red–ox state.

In the case of an oxidized sample, nitrates formation resulted approximately in a ratio of three moles of NO_2 consumed for one mole of NO released, in line with the stoichiometry associated with a two-step mechanism involving first disproportionation of NO_2 to form surface nitrites and nitrates, followed by oxidation of nitrites by NO_2 to give more nitrate adspecies. In the case of a reduced sample, significantly higher NO evolution and nitrates storage were recorded upon exposure of the catalysts to NO_2, with significant practical implications. Coupling original gas-phase results presented in this work with spectroscopic evidence from the literature, we have explained the more copious NO evolution with the following picture: reduced species (either Fe or Cu), abundant on the catalyst surface after the reducing pre-treatment, are first oxidized by NO_2, with formation of NO according to a 1:1 stoichiometry; then, the classical two step NO_2 adsorption mechanism, based on NO_2 disproportionation, can take place over the oxidized species. The greater amount of stored nitrates observed on the pre-reduced sample was instead justified invoking the re-dispersion of Fe and Cu ions during the reduction phase, which thus provides additional sites for nitrates storage.

Acknowledgements

The financial support of Daimler AG is gratefully acknowledged. The Authors wish to thank Dr. Bernd Krutzsch, Dr. Michel Weibel and Dr. Volker Schmeisser for useful discussions.

Appendix A.

Dedicated NO_2 adsorption/TPD tests were performed in the absence of the catalyst, with the micro-reactor totally filled with corundum particles only (indicated as "blank reactor" in the following). Fig. A1 shows species outlet concentrations during a temperature ramp performed over the blank reactor after exposure to 1000 ppm of NO_2 at 200 °C. It is evident that above 400–450 °C a significant amount of NO_x was released from the reactor. A quantitative analysis indicated that the amount of NO_x released during tests in the blank reactor was comparable to the amount measured at temperatures above 450 °C during similar tests performed in the presence of either the Fe-zeolite or the Cu-zeolite catalyst. More blank runs were also performed replacing corundum as filler with quartz grains: this resulted in the absence of any NO_x adsorption/desorption above 450 °C (see e.g. Fig. 4B). It appears therefore that the NO_x desorption feature observed in our runs above 450 °C was a spurious contribution due to NO_2 adsorption on the corundum filler of the reactor.

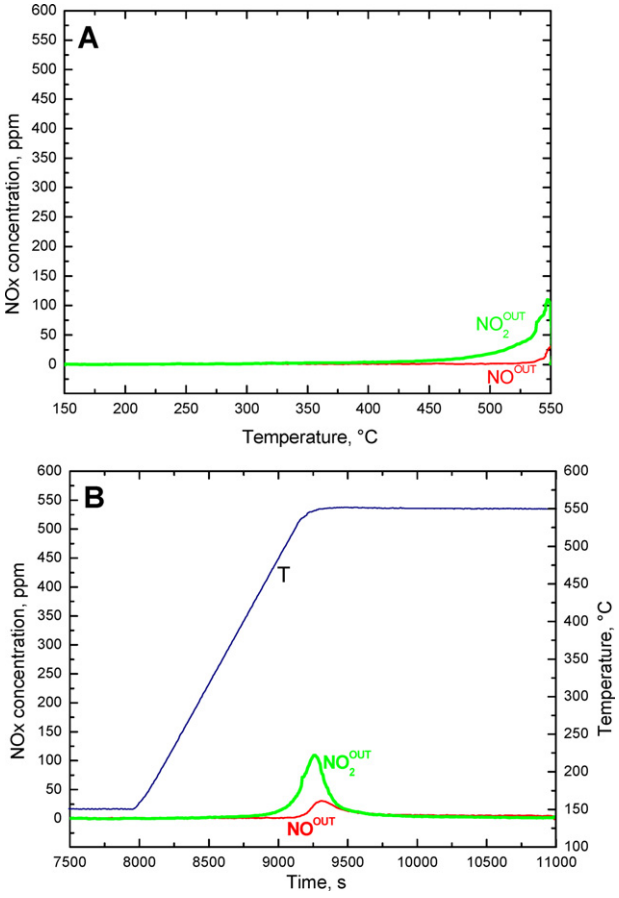

Fig. A1. NO_2 TPD in "blank reactor" (corundum only). Adsorption phase (not reported): T = 200 °C, Q = 71 cm^3/min (STP), NO_2 = 1000 ppm, carrier gas = He; TPD: T-ramp = 20 K/min, Q = 71 cm^3/min (STP), He flow. (A) NO and NO_2 concentrations as a function of reactor temperature. (B) NO and NO_2 concentrations as a function of time.

References

[1] T.V. Johnson, SAE Technical Papers 2010-01-0301.
[2] P. Forzatti, L. Lietti, E. Tronconi, Encyclopedia of Catalysis, Wiley, New York, 2003, pp. 298–343.
[3] M. Ahrens, O. Marie, P. Bazin, M. Daturi, Journal of Catalysis 271 (2010) 1–11.
[4] T. Ibusuki, K. Takeuchi, Journal of Molecular Catalysis 88 (1994) 93–102.
[5] T. Maggos, J.G. Bartzis, P. Leva, D. Kotzias, Applied Physics A: Materials Science & Processing 89 (2007), 81-84-84.
[6] M.-C. Wu, N.A. Kelly, Applied Catalysis B: Environmental 18 (1998) 79–91.
[7] N. Apostolescu, T. Schröder, S. Kureti, Applied Catalysis B: Environmental 51 (2004) 43–50.
[8] I. Nova, L. Castoldi, L. Lietti, E. Tronconi, P. Forzatti, F. Prinetto, G. Ghiotti, Journal of Catalysis 222 (2004) 377–388.
[9] J. Despres, M. Koebel, O. Kröcher, M. Elsener, A. Wokaun, Applied Catalysis B: Environmental 43 (2003) 389–395.
[10] M. Iwasaki, H. Shinjoh, Journal of Catalysis 273 (2010) 29–38.
[11] J.n. Szanyi, J.H. Kwak, C.H.F. Peden, The Journal of Physical Chemistry B 108 (2004) 3746–3753.
[12] K. Hadjiivanov, D. Klissurski, G. Ramis, G. Busca, Applied Catalysis B: Environmental 7 (1996) 251–267.
[13] M. Iwasaki, H. Shinjoh, Physical Chemistry Chemical Physics 12 (2010) 2365–2372.
[14] H. Sjövall, E. Fridell, R. Blint, L. Olsson, Topics in Catalysis 42–43 (2007) 113–117.
[15] J. Szanyi, M.T. Paffett, Journal of Catalysis 164 (1996) 232–245.
[16] Z.-M. Wang, T. Arai, M. Kumagai, Industrial & Engineering Chemistry Research 40 (2001) 1864–1871.

[17] M. Rivallan, G. Ricchiardi, S. Bordiga, A. Zecchina, Journal of Catalysis 264 (2009) 104–116.
[18] A. Savara, A. Danon, W.M.H. Sachtler, E. Weitz, Physical Chemistry Chemical Physics 11 (2009) 1180–1188.
[19] A. Savara, W.M.H. Sachtler, E. Weitz, Applied Catalysis B: Environmental 90 (2009) 120–125.
[20] A. Savara, E. Weitz, The Journal of Physical Chemistry C 114 (2010) 20621–20628.
[21] E. Tronconi, I. Nova, M. Colombo, Industrial & Engineering Chemistry Research 49 (2010) 10374–10385.
[22] A. Grossale, I. Nova, E. Tronconi, Journal of Catalysis 265 (2009) 141–147.
[23] M. Colombo, I. Nova, E. Tronconi, Catalysis Today 151 (2010) 223–230.
[24] S.F. Yin, B.Q. Xu, X.P. Zhou, C.T. Au, Applied Catalysis A: General 277 (2004) 1–9.
[25] S.-F. Yin, Q.-H. Zhang, B.-Q. Xu, W.-X. Zhu, C.-F. Ng, C.-T. Au, Journal of Catalysis 224 (2004) 384–396.
[26] C. Ciardelli, I. Nova, E. Tronconi, D. Chatterjee, B. Bandl-Konrad, M. Weibel, B. Krutzsch, Applied Catalysis B: Environmental 70 (2007) 80–90.
[27] E. Tronconi, I. Nova, C. Ciardelli, D. Chatterjee, M. Weibel, Journal of Catalysis 245 (2007) 1–10.
[28] C. Ciardelli, I. Nova, E. Tronconi, M. Ascherfeld, W. Fabinski, Topics in Catalysis 42–43 (2007) 161–164.
[29] C. Ciardelli, I. Nova, E. Tronconi, B. Konrad, D. Chatterjee, K. Ecke, M. Weibel, Chemical Engineering Science 59 (2004) 5301–5309.
[30] A. Grossale, I. Nova, E. Tronconi, Catalysis Today 136 (2008) 18–27.
[31] M. Devadas, O. Kröcher, M. Elsener, A. Wokaun, N. Söger, M. Pfeifer, Y. Demel, L. Mussmann, Applied Catalysis B: Environmental 67 (2006) 187–196.
[32] S. Brandenberger, O. Kroecher, A. Tissler, R. Althoff, Catalysis Reviews: Science and Engineering 50 (2008) 492–531.
[33] M. Santhosh Kumar, M. Schwidder, W. Grünert, U. Bentrup, A. Brückner, Journal of Catalysis 239 (2006) 173–186.
[34] G. Li, C.A. Jones, V.H. Grassian, S.C. Larsen, Journal of Catalysis 234 (2005) 401–413.
[35] M. Devadas, O. Kröcher, M. Elsener, A. Wokaun, G. Mitrikas, N. Söger, M. Pfeifer, Y. Demel, L. Mussmann, Catalysis Today 119 (2007) 137–144.
[36] V. Sanchez-Escribano, T. Montanari, G. Busca, Applied Catalysis B: Environmental 58 (2005) 19–23.
[37] Z.-X. Gao, Q. Sun, W.M.H. Sachtler, Applied Catalysis B: Environmental 33 (2001) 9–23.
[38] R.Q. Long, R.T. Yang, Journal of Catalysis 198 (2001) 20–28.
[39] C. England, W.H. Corcoran, Industrial & Engineering Chemistry Fundamentals 13 (1974) 373–384.
[40] M. Iwasaki, K. Yamazaki, K. Banno, H. Shinjoh, Journal of Catalysis 260 (2008) 205–216.
[41] Y. Yeom, M. Li, A. Savara, W. Sachtler, E. Weitz, Catalysis Today 136 (2008) 55–63.
[42] K.-i. Segawa, Y. Chen, J.E. Kubsh, W.N. Delgass, J.A. Dumesic, W.K. Hall, Journal of Catalysis 76 (1982) 112–132.
[43] K. Hadjiivanov, J. Saussey, J.L. Freysz, J.C. Lavalley, Catalysis Letters 52 (1998) 103–108.
[44] R. Kefirov, E. Ivanova, K. Hadjiivanov, S. Dzwigaj, M. Che, Catalysis Letters 125 (2008) 209–214.
[45] G. Mul, J. Pérez-Ramírez, F. Kapteijn, J.A. Moulijn, Catalysis Letters 80 (2002) 129–138.
[46] L.J. Lobree, I.-C. Hwang, J.A. Reimer, A.T. Bell, Journal of Catalysis 186 (1999) 242–253.
[47] S.C. Larsen, A. Aylor, A.T. Bell, J.A. Reimer, The Journal of Physical Chemistry 98 (1994) 11533–11540.
[48] D.L. Hoang, T.T.H. Dang, J. Engeldinger, M. Schneider, J.R. Radnik, M. Richter, A. Martin, Journal of Solid State Chemistry 184 (2011) 1915–1923.
[49] R. Bulánek, B. Wichterlová, Z. Sobalìk, J. Tichý, Applied Catalysis B: Environmental 31 (2001) 13–25.
[50] B. Wichterlová, Z. Sobalík, J. Dědeček, Catalysis Today 38 (1997) 199–203.